

THE ROLE OF FRICTION AND NONLINEAR ELASTICITY DURING PULL-OFF OF PRESSURE SENSITIVE ADHESIVES

Nicholas J. Glassmaker¹, Costantino Creton², Chung-Yuen Hui³

1. Central Research & Development, E.I. DuPont de Nemours & Co., Wilmington, DE 19880-0400
2. Laboratoire de Physique des Polymères et Milieux Dispersés, ESPCI, 75231 Paris Cedex 05, France
3. Dept. of Theoretical & Applied Mechanics, Cornell University, Ithaca, NY 14853

e-mail: 1. Nicholas.J.Glassmaker@usa.dupont.com, 2. Costantino.Creton@espci.fr, 3. ch45@cornell.edu

Introduction

Pressure sensitive adhesives (PSAs) are typically soft materials, composed of a blend of polymers, with both elastic and dissipative aspects. When a thin film of a PSA is placed under lateral tension, a large hydrostatic tension in the film leads to cavity formation and growth. Subsequently, walls between cavities form thin fibril-like structures that can extend to very large stretch ratios. While this occurs, an extended “foot” region at the bottom of each fibril remains in contact with the substrate. The behavior of the foot during fibril stretching plays an important role in determining the performance of the PSA, as measured by the sustained tensile force, maximum tensile strain, and amount of energy dissipation. In many cases, the foot is observed experimentally to fail in a sliding mode. A mechanical model of this phenomenon is presented which considers velocity dependent friction at the interface and nonlinear elasticity or viscoelasticity with finite extensibility in the fibril. A finite difference method is employed to solve the governing equations. Detailed results regarding the strain to failure and stress versus nominal strain in the fibrillar structures are given. The results are shown to depend on several factors, including the velocity at which the fibril is pulled, frictional resistance, and details of the nonlinear elastic constitutive behavior in the fibril. We present new experimental data showing how the contact foot evolves and compare this with the results of our model.

Experimental

In the tack test (Fig. 1), a rigid flat cylindrical punch is brought into contact with a thin layer of PSA. After intimate contact is established, the punch is retracted. During retraction, cavities typically nucleate at defects along the interface and expand into the PSA film to increase the compliance of the layer. Once the cavities grow to be roughly the same size as the film thickness, they cannot expand further without encountering neighboring cavities. However, the walls between cavities continue to be stretched in the direction of the applied force. After some deformation, the inter-cavity walls comprise a web of thin fibril-like structures which can be extended to very large stretch ratios.

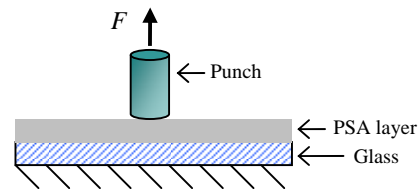


Fig. 1. Schematic diagram of the tack test. Observation is from below in this view.

During the fibril stretching phase of PSA failure, close inspection of the contact interface shows that the contact area initially extends far beyond the stretched walls into the neighboring cavities. The geometry is shown schematically in Fig. 2c, where we have labeled the extended contact region as a “foot.” As the stretch (and stress) in the fibril increases with continuing deformation, we have observed that the contact foot recedes in a stable way. By analyzing sequences of images such as those shown in Fig. 3, the displacement of the edge of the foot was found as a function of time. Typical results are shown in Fig. 4.

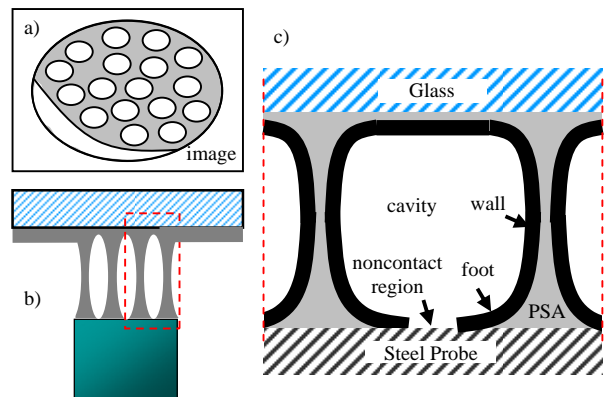


Fig. 2. Schematic diagram of a) the end-view image observed in the microscope of the tack apparatus, b) macroscopic side-view of the stretched, fibrillated film, and c) zoomed side-view of the detailed shape of the fibrils, cavity, and contacting feet within the dashed box of Fig. 2b.

It is quickly evident from Fig. 4 that the foot moves at a constant speed. However, the speed appears to vary from cavity to cavity and sample to sample, even though the cavities were chosen randomly and all other experi-

mental conditions were kept identical. This probably has to do with the fact that cavities are asymmetrically shaped, so that the feet of different cavities, indeed the feet of the different regions of the same cavity, are positioned at different orientations and distances relative to the nearest wall.

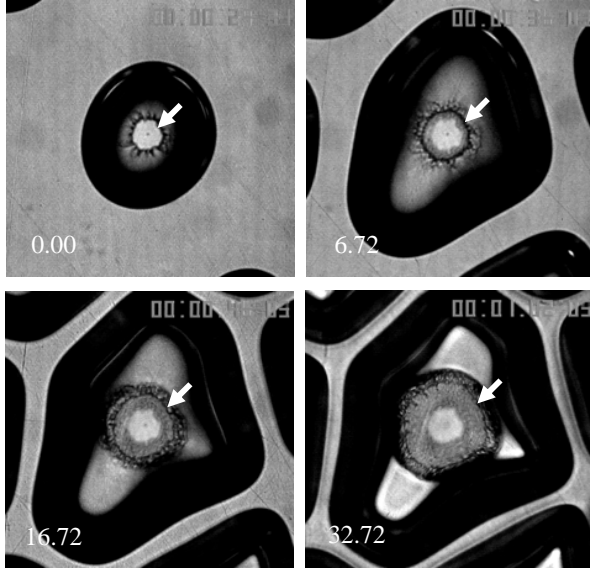


Fig. 3. Sequence of images showing the motion of the contacting foot interior to a cavity just after the cavity reaches its maximum lateral size. As the walls between cavities are stretched in the last 3 images, the foot migrates significantly toward the walls. The contact line is indicated with a white arrow in each photo. The probe is separated from the PSA film at a constant rate of $10 \mu\text{m/s}$. White numbers indicate the time relative to the initial image.

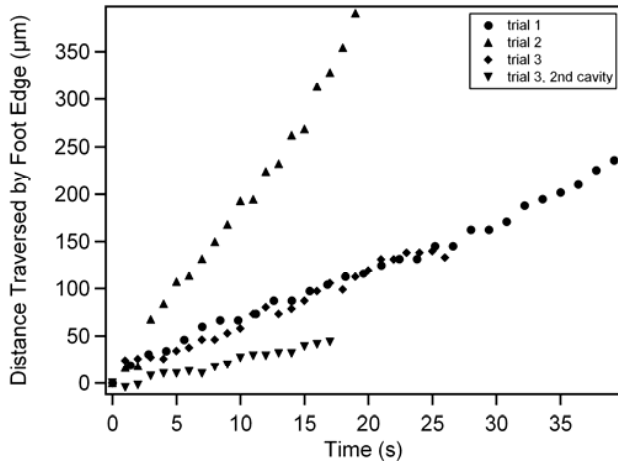


Fig. 4. Typical results for the displacement of the edge of the foot as a function of time. The experimental images of Fig. 3 correspond to “trial 1” in this plot.

In spite of these differences, the overall behavior appears to be qualitatively similar in all cases observed: feet are pulled in a sliding mode relative to the flat steel probe

surface. The driving force for this motion is tension in the fibril, which is transferred to the foot via the curved geometry of the material connecting the fibril and foot. Interfacial friction resists this motion. In the next section we present a simplified mechanical model of this phenomenon. Through the model, we seek to provide qualitative understanding about which experimental and material parameters control the foot sliding process. For example, we show that changing material properties can have a significant effect on the strain to failure, maximum stress, and foot speed.

Theoretical Model (Elastic Case)

An idealization of the wall and foot geometry which we propose to model the foot sliding phenomenon is shown in Fig. 5a. We assume that the foot is subject to a generic frictional shear stress (Fig 5b) which depends linearly on the local velocity of sliding. The only other force on the element of the foot in Fig. 5b is the internal tension.

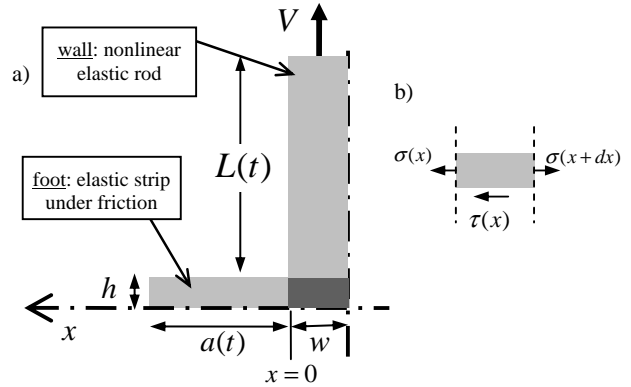


Fig. 5. Diagram showing the simplified model of the wall and foot geometry: a) geometric variables, b) free body diagram of the forces on an element of the foot.

This shear-lag model of friction in the foot leads to the following governing equation

$$\frac{\partial \bar{u}}{\partial \bar{t}} = \frac{\partial^2 \bar{u}}{\partial \bar{x}^2}, \quad (1)$$

and initial and boundary conditions

$$\bar{u}(\bar{x}, 0) = 0, \quad (2)$$

$$\frac{\partial \bar{u}}{\partial \bar{x}}(1, \bar{t}) = 0, \quad (3)$$

$$\frac{\partial \bar{u}}{\partial \bar{x}}(\hat{x}, \bar{t}) = \begin{cases} \frac{2\omega(1 + \lambda^{-1}\Xi)(\lambda - \lambda^{-2})}{3(1 + \Xi)}, & (\text{M-R}) \\ \frac{\omega(\lambda - \lambda^{-2})}{3(1 - (\lambda^2 + 2/\lambda - 3)/J_m)}. & (\text{Gent}) \end{cases} \quad (4)$$

Here, the normalization is such that $\bar{u} = u/a_0$, $\bar{x} = x/a_0$, and $\bar{t} = t/(a_0^2 \gamma/Eh)$, where $a_0 = a(0)$ is the initial foot length, E is the small strain modulus, and γ is the constant

relating the frictional shear stress to the local velocity of the foot. In addition,

$$\lambda = \frac{1 + \Omega \bar{t}}{1 + \hat{x} \mu / \omega}, \quad (5)$$

is the stretch in the fibril, and \hat{x} is such that

$$\bar{u}(\hat{x}, \bar{t}) = \hat{x}. \quad (6)$$

In equation (4), “M-R” is indicated next to the normalized Mooney-Rivlin constitutive law [1], which represents softening relative to neo-Hookean behavior. In (4), Ξ is a normalized parameter equal to the ratio of C_2 to C_1 . Meanwhile, “Gent” refers to the hardening constitutive law [2] which blows up in stress and stored elastic energy at a limiting value J_m of the first strain invariant. Note that eq. (4) assumes the stress on the fibril is identical to that applied horizontally to the foot.

Several values of the material parameters Ξ and J_m were explored, while geometric parameters μ and ω were held constant at reasonable values for the observed fibril and foot geometry. The experimental control parameter Ω (eq. (5)) corresponds to the normalized speed of pulling the fibril and was varied over a wide range. Results are shown in Figs. 6 and 7.

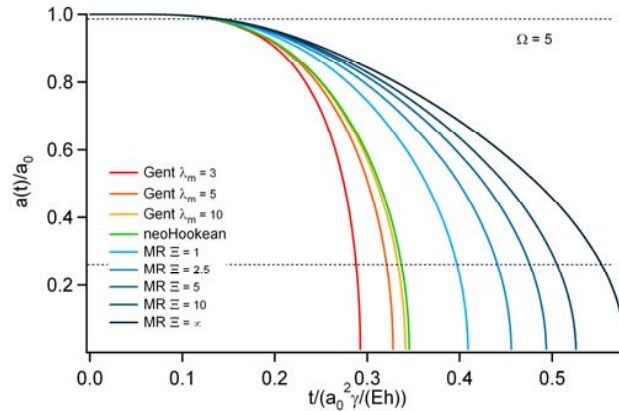


Fig. 6. Simulation results for the evolution of the foot size for one selected normalized pull speed and the range of elastic materials studied. Dashed lines roughly indicate the part of the results that one can typically measure in experiments.

Discussion

In Fig. 6, the evolution of the size of the foot is shown for one case of the normalized pull speed Ω . The initially stationary foot accelerates throughout the simulation as the strains and stresses slowly increase in the fibril and diffuse into the foot. Each material has a different acceleration rate, depending on its behavior at large strains. Unsurprisingly, the Gent materials accelerate fastest, as the stresses mount quickly when the fibril approaches the limit strain. Examination of similar results at other normalized pull

speeds are also self-consistent in that the foot fails more quickly for all materials at larger Ω , and vice versa for smaller Ω . This self-consistency is reassuring, but comparison with experiment reveals some differences. Most notably, the results in Fig. 4 show that foot motion appears to occur at constant velocity, even though local differences in geometry change the quantitative value of that velocity. A partial explanation for this difference is that experimental limitations limit the range over which foot motion is visible, as indicated by the dashed lines in Fig. 6. Within the dashed lines, the velocity changes less, but this does not fully explain this inconsistency between the model and experiment.

Moving on, in Fig. 7 one sees that the failure strain increases in a power law fashion for normalized pull speed less than about 1, regardless of the material. In this low speed, low friction condition, the detachment behavior is controlled by the friction coefficient rather than by the nonlinear properties of the fibril. However, at larger values of Ω , material differences become important. Notably, Gent type materials which harden as they reach a given value of J_m , reach a plateau strain at the corresponding λ_m , since the stresses blow up at this strain. On the other hand, Mooney-Rivlin materials do not exhibit this behavior. Depending on the value of Ξ , i.e. the amount of softening relative to a neoHookean material, very large maximal strains are possible, and these continue to increase with increasing Ξ . In practice the total work to reach total detachment will be significantly higher for these cases.

The relevance of these results to classes of PSA materials will be explored further in the talk, and a viscoelastic version of the model will also be presented that space limitations prevent here.

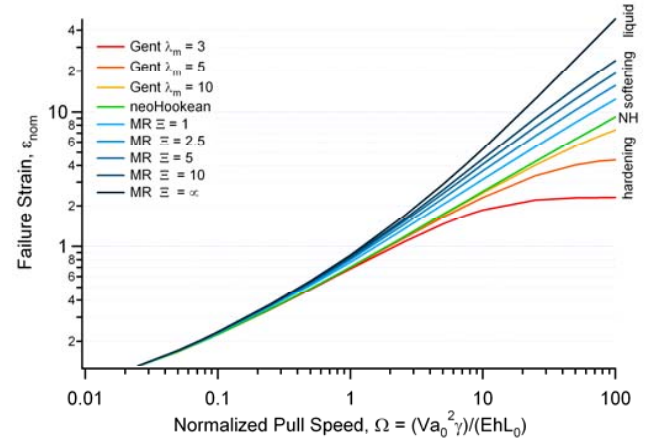


Fig. 7. Simulation results for the failure strain in the fibril, i.e. the strain when the foot has been 99% transferred to the fibril, shown as a function of the normalized speed.

References

1. Treloar, L. R. G., *The Physics of Rubber Elasticity*. 3rd ed.; Oxford Univ. Press: Oxford, 1975.
2. Gent, A. N., *Rubber Chemistry and Technology* **1996**, 69, 59-61.